EurJIC
European Journal of Inorganic Chemistry

Full Paper
doi.org/10.1002/ejic.202000727

Chemistry Europe
European Chemical Societies Publishing

Nickel Pincer Complexes

Enhancing the Stability of Aromatic PCN Pincer Nickel Complexes by Incorporation of Pyridine as the Nitrogen Side Arm

Abdelrazek H. Mousa,[a] Kaushik Chakrabarti,[a] Ghodsieh Isapour,[a] Jesper Bendix,[b] and Ola F. Wendt*[a]

Abstract: New PCN^{Py} pincer nickel complexes have been synthesized through a short synthetic route. Incorporating pyridine as the nitrogen side arm facilitated the C–H activation in the PCN ligand and allowed the cyclometallation with nickel to take place at room temperature. Pyridine also enhanced the stability of β-hydrogen-containing alkyl complexes. Also, the symmetric NCN nickel complex with pyridine side arms was successfully obtained giving a rare example of such type of complexes to be prepared through direct C–H activation. Furthermore, preliminary results showed that the (PCN^{Py})Ni–Br is active in Kumada coupling reactions particularly the coupling of aryl halides with aryl Grignard reagents.

Introduction

Despite the fast expansion of the field of pincer complexes,[1–9] those with unsymmetric pincer ligands have received limited attention compared to the symmetric ones in part as a result of the long synthetic routes used to prepare the unsymmetric ligand scaffolds.[10–23] However, unique reactivity has sometimes been documented for these ligands, and for PCN ligands such reactivity includes selective C–C vs. C–H bond activation and hemilability through de-coordination of the weak side arm of the unsymmetric pincer ligand.[10–12,18] Also increased reactivity in CO_2 insertion has been reported.[23] The hemilability of unsymmetric pincer complexes is sometimes important but it also counteracts the stability of these complexes and can facilitate their decomposition, as reported by us and others for PCN pincer complexes.[12,18,22] Introducing a relatively strongly binding nitrogen side arm could enhance the stability of the PCN complexes. Pyridine has been widely used as a directing group in C–H functionalization reactions due to its strong ability to bind to the metal center, which facilitates the C–H activation step and/or stabilizes the product.[24–30] Here, we report the synthesis of a new (PCN^{Py})H pincer ligand bearing pyridine as the nitrogen side arm. The pyridine arm is installed in one synthetic step through a cross-coupling reaction which is a great advantage in that it gives facile accessibility to an unsymmetric pincer ligand. Cyclometallation of the new (PCN^{Py})H ligand with nickel offered the corresponding nickel complexes at room temperature and enabled the synthesis of the corresponding ethyl complex, which was structurally characterized. The advantage of using pyridine was also exploited to cyclometallate the NCN pincer ligand enabling a straightforward synthesis of the NCN nickel complex. The reactivity of the $^{t\text{Bu}}$PCN^{Py} nickel complex in Kumada coupling reactions was investigated giving promising results.

[a] Dr. A. H. Mousa, Dr. K. Chakrabarti, G. Isapour, Prof. O. F. Wendt
Centre for Analysis and Synthesis, Department of Chemistry,
Lund University,
P. O. Box 124, 221 00 Lund, Sweden
E-mail: ola.wendt@chem.lu.se
[b] Prof. J. Bendix
Department of Chemistry, University of Copenhagen,
Universitetsparken 5, 2100 Copenhagen, Denmark
Supporting information and ORCID(s) from the author(s) for this article are available on the WWW under https://doi.org/10.1002/ejic.202000727.
This manuscript is part of the Special Collection Pincer Chemistry and Catalysis.

Results and Discussion

Synthesis of ^{R}PCN^{Py} Ligands

Palladium-catalyzed Suzuki–Miyaura cross-coupling reaction of the two commercially available substrates, 2-bromopyridine (**1**) and 3-hydroxymethylphenyl boronic acid (**2**), allowed a straightforward construction of the nitrogen side arm of the PCN ligand.[30,31] In order to install the phosphine arm, the resulting cross-coupling product, 2-(3-hydroxymethylphenyl) pyridine (**3**), was treated with aqueous HBr to form the corresponding hydrobromide salt and subsequently, a nucleophilic substitution reaction with a secondary phosphine in the presence of Et_3N was carried out, see Scheme 1.

The ligands were characterized by NMR spectroscopy. A ^{31}P NMR spectrum of **4**[32] displayed a sharp singlet peak at 33.35 ppm similar to our previously reported $^{t\text{Bu}}$PCN^{Me} analog.[18] Changing the substituents on the phosphorus donor atom has a great influence on the ^{31}P chemical shift and in ligand **5** the ^{31}P NMR signal resonates at a higher field (1.94 ppm) compared to **4**.

Full Paper
doi.org/10.1002/ejic.202000727

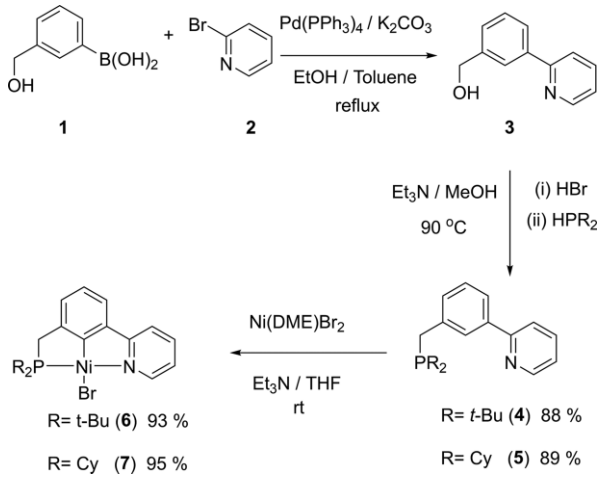

Scheme 1. Synthesis of $^{R}PCN^{Py}$ ligand and the corresponding (PCN)Ni-Br complexes.

Synthesis of $^{R}PCN^{Py}$ Nickel Complexes

Addition of Ni(DME)Br_2 (DME = 1,2-dimethoxyethane) to a solution of ligand **4** in THF followed by addition of ten equivalents of Et_3N resulted in immediate formation of a golden yellow solution and a white precipitate at room temperature. NMR spectroscopy was used to probe the structure of the yellow compound after workup. The presence of a singlet peak at 85.85 ppm in the ^{31}P NMR spectrum in addition to the downfield shift observed in the ^{1}H NMR spectrum for the phosphorus side arm protons ((*t*Bu)$_2$ and CH_2P) compared to that of the ligand strongly supports the metallation of ligand **4**. The structure of the new complex, **6**, was confirmed using X-ray diffraction analysis, and the molecular structure is given in Figure 1. Overall, complex **6** displayed similar NMR features as our previously published PCN^{Me} nickel bromide complex.[22] The ^{31}P NMR chemical shift is almost the same for both complexes. Furthermore, the *tert*-butyl groups appear at the same ^{1}H NMR chemical shift. To investigate the influence of the substituents of the phosphorus donor on the cyclometallation reaction, the analogous ligand **5** was treated with Ni(DME)Br_2 using the same

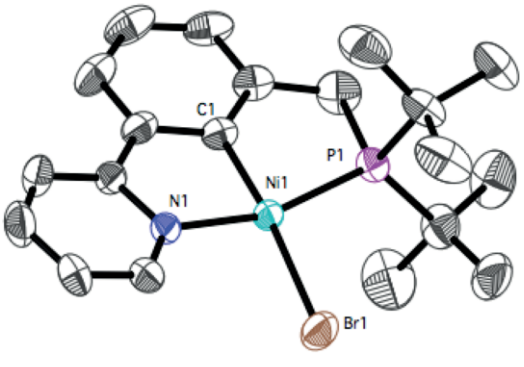

Figure 1. Molecular structures of complex **6** at the 50 % probability level. Hydrogen atoms are omitted for clarity. Selected bond lengths [Å] and bond angles (°): Ni1–C1 = 1.881(3), Ni1–P1 = 2.1767(10), Ni1–N1= 1.977(3), Ni1–Br1 = 2.3690(6), C1–Ni1–Br1 = 170.85 (10), C1–Ni1–P1 = 83.35 (11), C1–Ni1–N1 = 83.67 (14), N1–Ni1–P1 = 162.92 (8), P1–Ni1–Br1 = 100.02 (3), N1–Ni1–Br1 = 94.50(8).

reaction conditions. This gave complex **7** suggesting facile cyclometallation irrespective of the substituents on the phosphorus donor atom. The structure of **7** was confirmed with X-ray diffraction analysis and the molecular structure is given in Figure 2. All reactions are shown in Scheme 1. The facile cyclometallation is probably due to the strong chelation of both the phosphine and the pyridine side arms. Pyridine is well known as a common directing group that enhances cyclometallation and selective C–H functionalization reactions.[24–28]

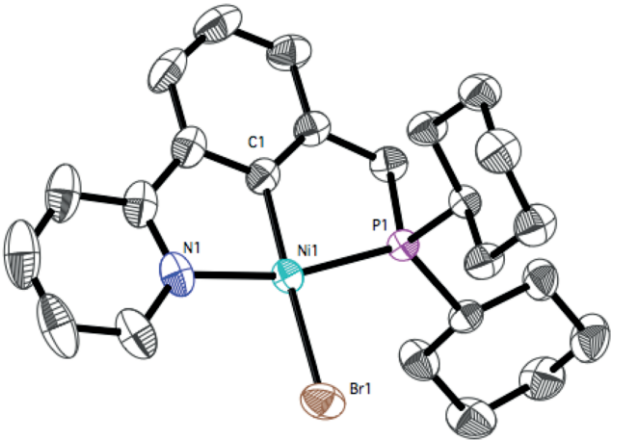

Figure 2. Molecular structures of complex **7** at the 50 % probability level. Hydrogen atoms are omitted for clarity. Selected bond lengths [Å] and bond angles (°): Ni1–C1 = 1.878(3), Ni1–P1 = 2.1465(7), Ni1–N1= 1.977(2), Ni1–Br1 = 2.3723(4), C1–Ni1–Br1 = 178.34 (9), C1–Ni1–P1 = 82.47 (9), C1–Ni1–N1 = 83.19 (11), N1–Ni1–P1 = 164.90 (8), P1–Ni1–Br1 = 95.92 (2), N1–Ni1–Br1 = 98.37(8).

Synthesis of NCN^{Py} Nickel Complexes

Given the mild conditions under which the PCN ligand underwent cyclometallation we were interested in investigating the corresponding symmetric NCN ligand (**8**), which was prepared using a Stille coupling reaction as described previously.[33] In this case, no cyclometallation with nickel precursors was observed at room temperature. This indicates that both the pyridine and phosphine arms are necessary to achieve a facile cyclometallation reaction. However, the cyclometallated NCN pincer nickel complex **9** was successfully obtained at 75 °C (Scheme 2).[34] This is a rare example of an NCN pincer nickel complex accessible through direct C–H activation. NCN pincer nickel complexes (Figure 3, **A**) were first reported by van Koten and are usually prepared either through an oxidative addition of the C–X bond of the halide functionalized NCN ligand using Ni(COD)$_2$ or a transmetallation of the lithiated NCN ligand with a Ni(II) precursor. The previous examples of direct C–H activation of an NCN ligand with nickel include imidazole or pyrazole nitrogen donors[35] and as is observed here sp^2-hydridization of the nitrogen seems favorable in inducing C–H activation. One possibility is that putting the nitrogen donor in a five- or six-membered ring makes for a sufficiently rigid coordination to put the C–H bond close to the nickel center. The structurally related CNN pincer nickel complex (Figure 3, **B**) has also been reported but the synthetic approach used is not straightforward and functionalization of the CNN ligand is required in order for

Full Paper
doi.org/10.1002/ejic.202000727

a successful cyclometallation through oxidative addition.[36] In the previous report of this ligand,[33] it was shown to readily cyclometallate to platinum whereas palladium precursors invariably gave different dinuclear products.

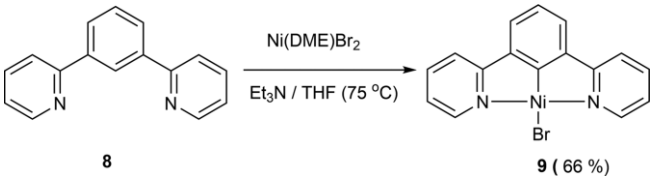

Scheme 2. Synthesis of (NCN)Ni-Br.

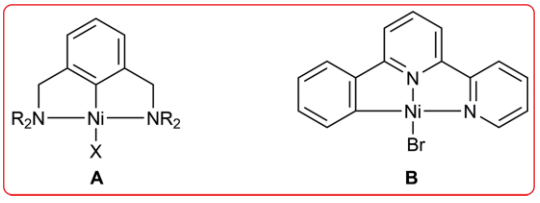

Figure 3. Structurally related NCN (CNN) nickel complexes.

The molecular structures of complex **9** were also corroborated using X-ray diffraction analysis, cf. Figure 4.[34] A square-planar geometry is adopted by the nickel center, which is common for the three complexes with different degrees of distortion, controlled by the side donor atoms of their ligand architectures. For complexes **6** and **7**, the substituents on the phosphorus donor significantly influence the bond angles and the bond lengths due to the difference in the steric hindrance between the *tert*-butyl groups and the cyclohexyl groups. For example, the P1–Ni1–Br1 in complex **6** is wider than that in complex **7** (100.02 (3) vs. 95.92 (2)). The same trend is observed for the C1–Ni1–P1 angles (83.35 (11) vs. 82.47 (9)). Changing the position of one of the nitrogen donor atoms from the center of the ligand scaffold in complex **B** to the side in complex **9** has a significant effect on the Ni-Br bond length. Elongation in the case of complex **9** is observed compared to the previously reported complex **B** (2.3989 (4) vs. 2.300 (1)) as a result of the higher trans influence of the central carbon atom of the NCN nickel complex vs. the central nitrogen atom of the CNN nickel complex.[34]

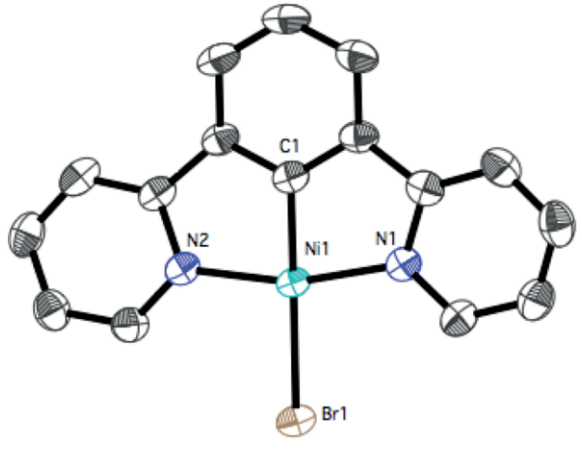

Figure 4. Molecular structures of complex **9** at the 50 % probability level. Hydrogen atoms are omitted for clarity. Selected bond lengths [Å] and bond angles (°): Ni1–C1= 1.827(3), Ni1–N1= 1.954(2), Ni1–N2= 1.951(2), Ni1–Br1= 2.3989(4), C1–Ni1–Br1= 179.53 (8), C1–Ni1–N1= 81.84 (10), C1–Ni1–N2= 81.89 (10), N1–Ni1–N2 = 163.73 (9), N1–Ni1–Br1 = 98.39 (6), N2–Ni1–Br1 = 97.88(6).

Complex **6** provided high valent nickel(III) species similar to our previously reported nickel halide complexes supported by the related PCN^{Me} pincer ligand.[22] Thus, the reaction of complex **6** with anhydrous $CuBr_2$ produced the corresponding nickel(III) complex, **10** (Scheme 3). In contrast to complex **6**, the symmetric NCN complex **9** failed to support high valent nickel(III) complexes under the same reaction conditions. This is rather surprising since the Ni(II)/Ni(III) oxidation potential for **6** is 0.27 V (vs. Fc/Fc$^+$, see supporting info for details) whereas the potential for **9** has been reported to be 0.16 V.[34] It means that although **9** is seemingly thermodynamically easier (in agreement with the expected increase in electron density) to

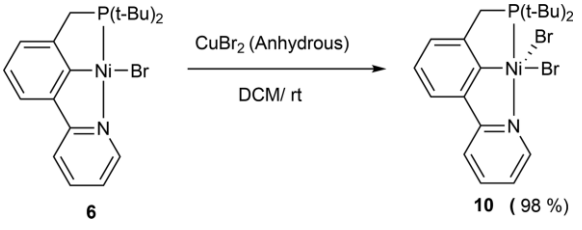

Scheme 3. Oxidation of complex **6**.

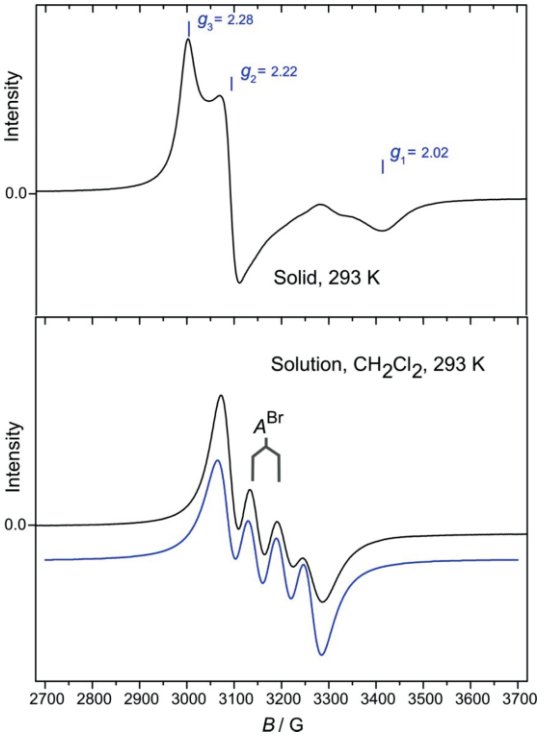

Figure 5. Top panel: experimental X-band EPR spectrum of undiluted **10** in the solid-state at r.t. The spectrum with *P*= 20 mW; modulation amplitude = 3.0 G, modulation freq. = 100 kHz. The g-values are reads off the spectrum and not simulated. Lower panel: X-band EPR spectrum and simulation (blue) of **10** in DCM solution at r.t. The spectrum was recorded with *P*= 6.325 mW; modulation amplitude = 2.0 G. Simulation parameters: g_{iso}= 2.167, $A^{Br}_{iso.}$ = 0.0060 cm^{-1}, Lorentzian derivative line shape, FWHH = 32 G.

Full Paper
doi.org/10.1002/ejic.202000727

oxidize there is a kinetic barrier towards chemical oxidation by $CuBr_2$. Complex **10** is NMR silent and the EPR spectrum of the solid at room temperature is shown in the upper panel of Figure 5. The featureless spectrum is interpretable as a rhombic S=1/2 spectrum with g_1 = 2.02, g_2 = 2.22, and g_2 = 2.28 ($g_{average}$ = 2.17). At room temperature, a dichloromethane solution gives an isotropic spectrum (g_{iso} = 2.17) with a resolvable hyperfine structure (A_{iso} = 0.0060 cm^{-1}) based on the strong coupling to one I = 3/2 nucleus (cf. Figure 5, lower panel). In agreement with previous reports,[22] this coupling must be a hyperfine coupling from the unpaired electron in the d_{z^2} orbital to a single bromide ligand showing that the solution structure is similar to the one in the solid-state. The strength of the coupling, which is more than 10 % of the hyperfine coupling in isolated bromine atoms,[37] indicates a pronounced covalency in the Ni-Br bonding. Magnetic susceptibility measurements show that the χT product behaves as expected for a low-spin d^7 system, providing a $g_{average} \approx 2.18$ in agreement with EPR results (cf. Figure S18). There is no indication of intermolecular interactions even at the lowest temperatures. In this respect, the system differs slightly from the previously studied system.[22]

Synthesis of a PCN Nickel Ethyl Complex

Our previously reported PCN^{Me} nickel platform failed to produce β-hydrogen-containing alkyl complexes due to facile β-elimination.[22] This is probably the result of the low steric hindrance of the methyl groups on the nitrogen donor and the potential hemilability of the amine arm which facilitates an agostic interaction that presumably precedes the β-elimination. The new PCN^{Py} complexes could potentially block such undesired decompositions and enhance the stability of the β-hydrogen-containing alkyl species due to the strong chelation of the pyridine to the nickel center. Thus, the reaction of complex **6** with EtMgCl was carried out at room temperature using C_6D_6 as solvent and the progress of the transmetallation reaction was followed by NMR spectroscopy. Gratifyingly, full conversion of complex **6** to the corresponding ethyl complex **11** was observed and the ethyl complex could be isolated and crystallized giving red crystals (Scheme 4). The molecular structure was determined using X-ray diffraction analysis (Figure 6). However, complex **11** is not completely thermally stable upon prolonged standing in C_6D_6 solution. At room temperature, within 5 h there is approximately 5 % decomposition of complex **11** to ligand **5** and Ni black particles. After 24 h, around 12 % of complex **11** was decomposed. It suggests that there is a slow β-hydrogen elimination forming a nickel hydride complex which undergoes reductive elimination to furnish ligand **5** and Ni(0) particles. This decomposition pathway is similar to the one suggested previously but substantially slower and will be the subject of further, more detailed investigations.

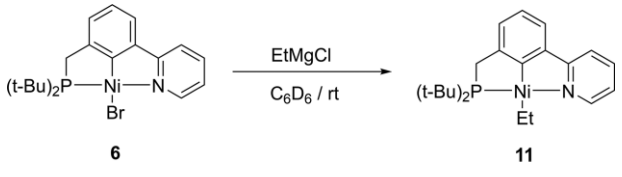

6 **11**

Scheme 4. Synthesis of ($^{R}PCN^{Py}$)Ni–Et (**11**).

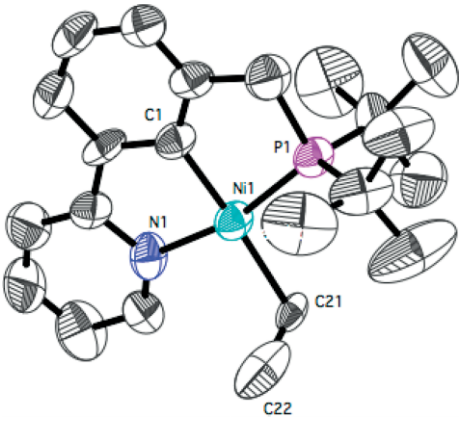

Figure 6. Molecular structures of complex **11** at the 50 % probability level. Hydrogen atoms are omitted for clarity. Selected bond lengths [Å] and bond angles (°): Ni1–C1= 1.899(15), Ni1–P1= 2.137(4), Ni1–N1= 1.991(12), Ni1–C21= 2.064(12), C1–Ni1–C21= 175.5 (6), C1–Ni1–P1= 83.0 (5), C1–Ni1–N1= 84.0 (6), N1–Ni1–P1 = 165.5 (4), P1–Ni1–C21 = 99.2 (4), N1–Ni1–C21 = 94.3(5).

Successful preparation and isolation of complex **11** encouraged us to study the reactivity of our new PCN nickel complexes in Kumada coupling reactions.

Catalytic Kumada Coupling Reaction

Our initial interest was to study the coupling of alkyl Grignard reagents with aryl halides (Table 1). Thus, the reaction of the EtMgCl with PhI was carried out in presence of 3 mol-% of complex **6**. 15 % yield of the cross-coupling product, ethylbenzene, was obtained based on GC analysis together with 8 % yield of the biphenyl as a homocoupling product (entry 1). Extending the reaction time to 24 h significantly enhanced the yield of the ethylbenzene (entry 2). Conducting the reaction at low temperature in order to quench the homocoupling formation led to a dramatic decrease in the yield of ethylbenzene (entry 3). The related PCN^{Me} nickel bromide complex was used as well but it also displayed a low reactivity at low temperature (entry 4).

Using PhCl as an electrophile instead of PhI gave no coupling product (entries 5 and 6). Employing the alkyl partner as the electrophile led to a significant decrease in the yield of the cross-coupling product and an increase of the undesired homocoupling product. The low reactivity of the PCN^{Me} nickel complex in the coupling of alkyl/aryl halides with aryl/alkyl Grignard reagents is in line with the unsuccessful preparation of the corresponding alkyl nickel complexes.[22] On the contrary, the reason for the observed low yield in the case of using complex **6** is not clear, but could also derive from the low thermal stability of the alkyl complex. It should be noted that we have not investigated the mechanism and can only speculate that **11** is involved in the catalytic cycle.

Next, we investigated the coupling of the aryl halides with aryl Grignard reagents (Table 2). 4-bromotoluene was employed as an electrophilic coupling partner and PhMgCl as the nucleo-

Full Paper
doi.org/10.1002/ejic.202000727

Table 1. Optimization of the reaction conditions of catalytic Kumada coupling reaction of aryl/alkyl halides and Et/PhMgCl.[a]

Entry	Alkyl/Ar-X	Alkyl/Ar-MgX	Catalyst	T [°C]	t [h]	Yield [%] Cross	Yield [%] Homo
1	PhI	EtMgCl	6	r.t.	7	15	8
2	PhI	EtMgCl	6	r.t.	24	26	6
3	PhI	EtMgCl	6	0	24	9	4
4	PhI	EtMgCl	(PCN^{Me})Ni-Br	0	24	12	4
5	PhCl	EtMgCl	(PCN^{Me})Ni-Br	r.t.	24	0	0
6	PhCl	EtMgCl	6	r.t.	24	0	0
7	*n*BuBr	PhMgCl	(PCN^{Me})Ni-Br	0	7	0	43
8	*n*BuBr	PhMgCl	6	0	7	0	31
9	*n*BuBr	PhMgCl	(PCN^{Me})Ni-Br	r.t.	24	3	27
10	*n*BuBr	PhMgCl	6	r.t.	24	3	25

[a] Reaction conditions: Alkyl/Aryl halide (0.25 mmol), Alkyl/ArylMgCl (0.3 mmol) and THF (3 mL). The yield was determined as an average of two runs by GC based on a calibration curve of the product using decane as internal standard.

Table 2. Optimization of the reaction conditions of catalytic Kumada coupling reaction of aryl halides and PhMgCl.[a]

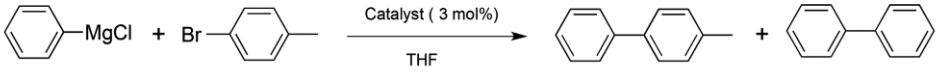

C H

Entry	Ar-X	Ar-MgX	Catalyst	T (°C)	t (h)	Additives	Additives (equiv.)	Yield (%) Cross	Yield (%) Homo
1		**PhMgCl**	**6**	rt	5			62	36
2	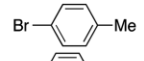	**PhMgCl**	**6**	rt	5	TMEDA	0.3	60	32
3	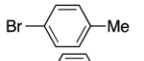	**PhMgCl**	**6**	rt	5	TMEDA	0.5	60	32
4	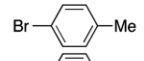	**PhMgCl**	**6**	rt	5	TMEDA	0.7	55	31
5	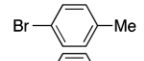	**PhMgCl**	**6**	rt	5	TMEDA	1	62	36
6	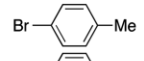	**PhMgCl**	**6**	rt	5	PPh_3	0.5	11	19
7	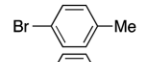	**PhMgCl**	**6**	rt	5	PPh_3	0.7	10	23
8	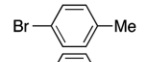	**PhMgCl**	**6**	rt	5	PPh_3	1	10	19
9[b]	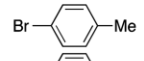	**PhMgCl**	**6**	rt	5			41	33
10	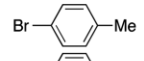	**PhMgCl**	**6**	0	5			59	35
11	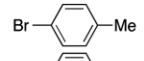	**PhMgCl**	**6**	-10	5			60	38
12	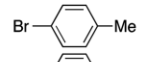	**PhMgCl**	**6**	-20	5			54	31
13	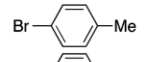	**PhMgCl**	**(PCN^{Me})Ni-Br**	rt	5			39	23
14	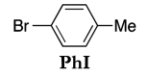	**PhMgCl**	**9**	rt	5			47	27
15[c]	**PhI**	**p-TolylMgCl**	**6**	rt	0.5			82	4

[a] Reaction conditions: Aryl halide (0.25 mmol), PhMgCl (0.3 mmol), and solvent (3 mL). The yield was determined as an average of two runs by GC based on a calibration curve of the product using mesitylene or decane as internal standard. [b] Toluene was used as solvent. Trace amount of 4,4′-dimethylbiphenyl was observed. [c] *p*-TolylMgCl was diluted by adding 3 mL of THF and the reaction was carried out for 30 minutes (8 % of 4,4′-dimethylbiphenyl was observed).

philic one. There was no cross-coupling product in absence of the catalyst.

Conducting the reaction in presence of 3 mol-% of the catalyst offered 62 % yield of the cross-coupling product, 4-methylbiphenyl with concomitant formation of 36 % of the homocoupling product, biphenyl, and trace amounts of the other homocoupling product, 4,4′-dimethylbiphenyl. In order to enhance the yield of the cross-coupling product, TMEDA was added as

Full Paper
doi.org/10.1002/ejic.202000727

it was previously reported by Hu to greatly enhance the yield of the cross-coupling product.[38] However, in our case there was no substantial change. PPh_3 led to a significant decrease in the yield of both the cross-coupling and homocoupling products. Using toluene instead of THF lowered the yield. Conducting the reaction at low temperatures gave almost the same results as at room temperature. The less sterically hindered PCN^{Me} nickel complex and the symmetric NCN complex **5** offered low reactivity compared to complex **3**. Conducting the catalytic reaction using a diluted solution of (*p*-tolyl)MgCl enhanced the yield of the cross-coupling product and allowed a short reaction time.

Conclusion

A slight modification of our previously reported PCN ligand by incorporation of a pyridine group as the nitrogen side arm instead of the NMe_2 gave a ligand that undergoes cyclometallation under very mild conditions and facilitates the synthesis of β-hydrogen-containing alkyl complexes. Furthermore, the incorporation of pyridine enabled an unusually short synthetic route to the PCN nickel complexes compared to previously reported examples. The symmetric (NCN)H ligand with two pyridine side arms was also synthesized and allowed, for the first time, for a direct cyclometallation with nickel precursors at fairly mild reaction conditions. The new PCN^{Py} complexes display a comparatively high reactivity in Kumada coupling reactions.

Experimental Section

General Procedures and Materials. All experiments were carried out under an inert atmosphere using glove box, Schlenk, or high vacuum line techniques unless otherwise noted. THF was vacuum transferred to the reaction vessel from sodium/benzophenone ketyl radical. Dry methanol was purchased from Sigma-Aldrich. Et_2O and DCM were obtained from an MBRAUN (MB-SPS 800) dry solvent dispenser. C_6D_6 was dried with and distilled from CaH_2. ^1H, $^{13}C\{^1H\}$, and $^{31}P\{^1H\}$ NMR spectra were recorded on a *Varian* Unity INOVA 500 spectrometer operating at 499.77 MHz (^1H) or a Bruker Avance 400 FT-NMR spectrometer operating at 400.1 MHz (^1H). Chemical shifts are given in ppm downfield from TMS using residual solvent peaks (^1H and ^{13}C) or H_3PO_4 (^{31}P) as reference. Multiplicities are abbreviated as follows: (s) singlet, (d) doublet, (t) triplet, (q) quartet, (m) multiplet. Elemental analyses were performed by H. Kolbe Microanalytisches Laboratorium, Mülheim an der Ruhr, Germany. The (NCN)H ligand was synthesized as previously reported.[33]

Synthesis of $[^{tBu}PCN^{Py}]H$ ligand 4. A Straus flask was charged with 329 mg (1 mmol) of 2-(3-bromomethylphenyl)pyridine•HBr salt. The flask was evacuated on the high vacuum line and introduced to the glove box where 15 mL of degassed and dry methanol was added followed by 0.37 mL (2 mmol) of di-*tert*-butyl phosphine. The flask was closed and removed from the glove box. The solution was stirred for 18 h at 100 °C. After allowing the mixture to cool down to room temperature, 1 mL dry triethylamine was added and it was stirred for 30 min. The volatiles were evaporated under high vacuum. The resulting sticky white solid was dissolved in degassed diethyl ether, filtered through Celite, and the filtrate was evaporated under high vacuum giving 276 mg (88 %) of the product as a colourless viscous liquid. ^1H NMR: δ = 8.60 (ddd, J = 4.7, 1.7, 0.9 Hz, 1H), 8.48 (s, 1H), 7.98 (d, J = 7.7 Hz, 1H), 7.47 (t, J = 8.5 Hz, 1H), 7.28 (t, J = 7.7 Hz, 1H), 7.09 (td, J = 7.7, 1.9 Hz, 1H), 6.64 (ddd, J = 7.4, 4.7, 0.9 Hz, 1H), 2.82 (d, $^2J_{HP}$ = 2.3 Hz, 2H,CH_2P), 1.07 (d, $^3J_{HP}$ = 10.6 Hz, 18H, $C(CH_3)_3$). $^{13}C\{^1H\}$ NMR: δ = 157.8 (s), 150.0 (s), 142.7 (d, $^2J_{CP}$ = 12.5 Hz), 139.8 (s), 136.3 (s), 130.8 (d, $^3J_{CP}$ = 9.4 Hz), 128.8 (s), 124.5 (d, $^3J_{CP}$ = 1.9 Hz), 121.9 (s), 120.2 (s), 31.8 (d, $^1J_{CP}$ = 24.2 Hz), 30.0 (d, $^2J_{CP}$= 13.6 Hz), 29.2 (d, $^1J_{CP}$ = 25.6 Hz). One aromatic carbon overlaps with the solvent signals. $^{31}P\{^1H\}$ NMR: δ = 33.3 (s).

Synthesis of $[^{Cy}PCN^{Py}]H$ ligand 5. A Straus flask was charged with 239 mg (0.73 mmol) of 2-(3-bromomethylphenyl)pyridine•HBr salt. The flask was evacuated on the high vacuum line and introduced to the glove box where 15 mL of degassed and dry methanol was added followed by 0.32 mL (1.45 mmol) of dicyclohexyl phosphine. The flask was closed and removed from the glove box. The solution was stirred for 18 h at 100 °C. After allowing the mixture to cool down to room temperature, 0.7 mL dry triethylamine was added and it was stirred for 30 min. The volatiles were evaporated under high vacuum. The resulting sticky white solid was dissolved in degassed diethyl ether, filtered through Celite, and the filtrate was evaporated under high vacuum and the flask was heated at 100 °C for 8 h to get rid of the excess of the dicyclohexyl phosphine and the dicyclohexyl phosphine oxide. The product was obtained as a colorless viscous liquid giving 236 mg (88.4 %). ^1H NMR: δ = 8.59 (d, J = 4.7 Hz, 1H), 8.41 (s, 1H), 7.98 (d, J = 7.7 Hz, 1H), 7.44 (d, J = 8.0 Hz, 1H), 7.40 (d, J = 7.4 Hz, 1H), 7.28 (t, J = 7.7 Hz, 1H), 7.09 (td, J = 7.7, 1.8 Hz, 1H), 6.64 (dd, J = 7.7, 4.8 Hz, 1H), 2.83 (s, 2H), 1.87–1.48 (m, 12H), 1.32–1.22 (m, 2H), 1.21–1.05 (m, 8H). $^{13}C\{^1H\}$ NMR: δ = 157.7 (s), 150.0 (s), 141.5 (d, $^2J_{CP}$ = 8.9 Hz), 140.0 (s), 136.3 (s), 130.4 (d, $^3J_{CP}$ = 7.4 Hz), 128.9 (s), 128.5 (d, $^3J_{CP}$ = 7.4 Hz), 124.6 (d, $^3J_{CP}$ = 2.0 Hz), 121.9 (s), 120.1 (s), 34.1 (d, $^1J_{CP}$ = 16.8 Hz), 30.3 (d, $^2J_{CP}$= 13.2 Hz), 29.8 (d, J_{CP} = 10.0 Hz), 27.7 (t, J_{CP} = 9.2 Hz), 26.9 (s). $^{31}P\{^1H\}$ NMR: δ = 1.94 (s).

Synthesis of $[^{tBu}PCN^{Py}]$Ni-Br (6). To a solution of ligand **4** (276 mg, 0.88 mmol) in 15 mL THF, (DME)$NiBr_2$ (271 mg, 0.88 mmol) was added inside the glovebox forming a greenish-white suspension, which changed to yellow upon stirring for 2 minutes with formation of a small amount of green solid. Then Et_3N (1.2 mL, 8.8 mmol) was added to the reaction mixture which immediately led to a complete change in colour to golden yellow. The flask was sealed and the reaction mixture stirred for 12 h at r.t. THF and all volatiles were removed under reduced pressure and the solid was dissolved in Et_2O, filtered through Celite and the solvent was evaporated under reduced pressure yielding 371 mg (93.5 %) of complex **6** as a crystalline yellow solid. Single crystals suitable for X-ray diffraction analysis were obtained from Et_2O at –20 °C. ^1H NMR (500 MHz, C_6D_6) δ 9.83 (d, J = 5.2 Hz, 1H), 6.99 (d, J = 4.2 Hz, 2H), 6.85 (d, J = 7.8 Hz, 2H), 6.77 (t, J = 7.5 Hz, 1H), 6.32 (t, J = 6.4 Hz, 1H), 2.88 (d, J = 8.9 Hz, 2H), 1.39 (d, J = 13.2 Hz, 18H). $^{13}C\{^1H\}$ NMR (126 MHz, C_6D_6) δ = 164.0 (d, J = 28.2 Hz), 163.6 (d, J = 1.9 Hz), 152.1 (s), 150.3 (d, J = 17.2 Hz), 147.4 (s), 138.1 (s), 125.2 (d, J = 16.8 Hz), 125.1 (s), 122.2 (d, J = 1.9 Hz), 120.6 (d, J = 1.5 Hz), 117.0 (s), 35.4 (d, J = 30.3 Hz), 35.0 (d, J = 14.2 Hz), 29.7 (d, J = 3.0 Hz). $^{31}P\{^1H\}$ NMR (202 MHz, C_6D_6) δ = 85.85 (s). Anal. Found (calcd. for. $C_{20}H_{27}BrNPNi$): C, 53.36 (53.26); H, 5.90 (6.03); N, 2.95 (3.11).

Synthesis of $[^{Cy}PCN^{Py}]$Ni-Br (7). To a solution of ligand **5** (236 mg, 0.64 mmol) in 15 mL THF, (DME)$NiBr_2$ (197 mg, 0.64 mmol) was added inside the glovebox forming a greenish-white suspension, which changed to yellow upon stirring for 2 minutes with formation of a small amount of green solid. Then Et_3N (0.9 mL, 6.4 mmol) was added to the reaction mixture which immediately led to complete change in colour to yellow. The flask was sealed and the reaction mixture stirred for 12 h at r.t. THF and all volatiles were removed

under reduced pressure and the solid was dissolved in Et_2O, filtered through Celite and the solvent was evaporated under reduced pressure yielding 305 mg (95 %) of complex **7** as a crystalline yellow solid. Single crystals suitable for X-ray diffraction analysis were prepared by slow diffusion of Et_2O into a DCM solution of **7** at 5 °C ^{1}H NMR (500 MHz, C_6D_6) δ 9.68–9.64 (m, 1H), 7.04–7.01 (m, 2H), 6.95–6.92 (m, 1H), 6.86 (d, *J* = 7.8 Hz, 1H), 6.77 (td, *J* = 7.7, 1.6 Hz, 1H), 6.34–6.29 (m, 1H), 2.79 (d, *J* = 9.1 Hz, 2H), 2.56 (d, *J* = 13.5 Hz, 2H), 2.11 (td, *J* = 12.1, 3.2 Hz, 2H), 1.84 (qdd, *J* = 12.9, 5.6, 3.8 Hz, 2H), 1.69 (d, *J* = 14.4 Hz, 2H), 1.61 (d, *J* = 13.0 Hz, 2H), 1.56–1.46 (m, 6H), 1.29–1.17 (m, 2H), 1.12–1.00 (m, 4H). ^{13}C{^{1}H} NMR (126 MHz, C_6D_6) *δ* = 165.9 (d, *J* = 29.7 Hz), 163.6 (d, *J* = 2.1 Hz), 151.9 (s), 149.9 (d, *J* = 18.6 Hz), 147.6 (d, *J* = 0.6 Hz), 138.2 (s), 125.6 (d, *J* = 18.1 Hz), 125.0 (s), 122.5 (d, *J* = 2.0 Hz), 120.9 (d, *J* = 1.6 Hz), 117.1 (s), 35.4 (d, *J* = 33.1 Hz), 34.5 (d, *J* = 23.0 Hz), 28.8 (dd, *J* = 14.2, 2.2 Hz), 27.1 (dd, *J* = 23.3, 11.4 Hz), 26.4 (d, *J* = 1.2 Hz). ^{31}P{^{1}H} NMR (202 MHz, C_6D_6) *δ* = 68.88 (s). Found (calcd. for. $C_{24}H_{31}BrNPNi$): C, 56.81 (57.30); H, 6.13 (6.21); N, 2.70 (2.78).

Synthesis of [NCN]Ni-Br (**9**). To a solution of the (NCN)H ligand **8** (441 mg, 1.9 mmol) in 35 mL THF, (DME)$NiBr_2$ (586 mg, 1.9 mmol) was added inside the glovebox. Then Et_3N (2.6 mL, 19 mmol) was added to the reaction mixture. The flask was sealed and the reaction mixture stirred overnight at 75 °C. THF and all volatiles were removed under reduced pressure and the solid was dissolved in DCM, washed with water, and the organic layer was dried with anhydrous Na_2SO_4. The solvent was evaporated under reduced pressure yielding 463 mg (65.8 %) of a reddish-yellow solid. Single crystals suitable for X-ray diffraction analysis were prepared by slow diffusion of Et_2O into a DCM solution of **9** at 5 °C. ^{1}H NMR (400 MHz, DMSO) δ 8.89 (d, *J* = 5.6 Hz, 2H), 8.07 (td, *J* = 7.7, 1.4 Hz, 2H), 7.93 (d, *J* = 7.7 Hz, 2H), 7.57 (d, *J* = 7.6 Hz, 2H), 7.39–7.30 (m, 2H), 7.23 (t, *J* = 7.6 Hz, 1H). ^{13}C{^{1}H} NMR (101 MHz, C_6D_6) *δ* = 168.8 (s), 162.1 (s), 154.1 (s), 144.1 (s), 140.3 (s), 125.3 (s), 123.5 (s), 123.2 (s), 119.0 (s). Anal. Found (calcd. for. $C_{16}H_{11}BrN_2Ni$): C, 51.80 (51.96); H, 3.13 (3.00); N, 7.49 (7.57).

Synthesis of [^{tBu}PCN^{Py}]Ni(III)Br$_2$ (10). To a solution of 18.04 mg (0.04 mmol) of **6** in 4 mL of DCM was added 8.93 mg (0.04 mmol) of anhydrous $CuBr_2$ immediately forming a deep red colored solution with concomitant formation of a precipitate. The reaction was left stirring for 1 h. Filtration over Celite and evaporation of the solvent under reduced pressure yielded 20.8 mg (98 %) of the product as dark crystalline solid. The complex is NMR silent. Anal. Found (calcd. for. $C_{20}H_{27}Br_2NPNi$): C, 45.52 (45.25); H, 5.27 (5.13); N, 2.61 (2.64).

Synthesis of [^{tBu}PCN^{Py}]Ni-Et (**11**). In a J. Young NMR tube, 20 μL (0.02 mmol, 2.0 M in THF) of EtMgCl was added to 9.0 mg (0.02 mmol) of complex **6** in 0.5 mL of C_6D_6 inside the glove box. The yellow colour of the solution turned immediately into red (wine). The reaction was monitored by ^{31}P{^{1}H} and ^{1}H NMR spectroscopy. The product was extracted with pentane and filtered through a short pad of Celite inside the glovebox. Single crystals suitable for X-ray diffraction analysis were obtained from pentane at –20 °C. ^{1}H NMR (500 MHz, C_6D_6) δ 8.64 (d, *J* = 5.6 Hz, 1H), 7.24 (d, *J* = 7.1 Hz, 1H), 7.15–7.08 (m, 3H), 6.93 (td, *J* = 7.9, 1.6 Hz, 1H), 6.48 (d, *J* = 6.5 Hz, 1H), 3.19 (d, *J* = 8.5 Hz, 2H), 1.60 (td, *J* = 7.8, 1.3 Hz, 3H), 1.28 (d, *J* = 12.3 Hz, 18H), 0.70 (qd, *J* = 7.8, 4.4 Hz, 2H). ^{13}C{^{1}H} NMR (101 MHz, C_6D_6) *δ* = 167.5 (d, *J* = 33.8 Hz), 167.4, 148.4, 138.9, 137.2, 124.2, 124.0, 123.6, 121.4 (d, *J* = 8.1 Hz), 119.7, 117.2, 39.6 (d, *J* = 29.2 Hz), 35.0 (d, *J* = 25.5 Hz), 29.6 (d, *J* = 15.1 Hz), 25.0, 14.2.^{31}P{^{1}H} NMR (202 MHz, C_6D_6) *δ* = 85.35 (s). Due to thermal decomposition the complex failed to give an accurate elemental analysis.

Magnetic measurements. The magnetic data were acquired on a Quantum-Design MPMS-XL SQUID magnetometer. Susceptibility data were acquired in a static field of 1.0 K Oe. Magnetization data were obtained with selected fields from 0 to 50 K Oe at *T* = 2–10 K in 1K intervals. The polycrystalline samples were measured on a compacted powder sample in a polycarbonate capsule. Data were corrected empirically for TIP and the diamagnetic contribution to the sample moment from the sample holder and sample was corrected through background measurements and Pascal constants, respectively.

EPR spectroscopy. The EPR spectra were recorded with a Bruker Elexsys E500 equipped with a Bruker ER 4116 DM dual-mode cavity, an EIP 538B frequency counter, and an ER035M NMR Gauss meter. Data were recorded at X-band frequencies (ν≈9.63 GHz). The spectra were simulated using home-written software considering an electronic spin of 1/2 and taking into account only the experimentally resolvable interactions with the nuclear spin of one bromide (*I* = 3/2). No distinction was made between the naturally occurring bromine isotopes. Simulation parameters are given in the Figure legends.

Electrochemical measurements. Cyclic voltammetry measurements were carried out at room temperature using a PalmSens potentiostat (–2 to +2 V for potential windows) and a 3mm glassy carbon electrode as working electrode, a Ag/AgCl leakless reference electrode, and a platinum wire as a counter electrode. A 1 mM solution of complex **6** in acetonitrile containing 0.1 M $(Bu_4N)PF_6$ as electrolyte was used and 0.1 V/s scan rate was applied. Ferrocene was used for standardization.

Crystallography. Data collection and refinement was performed as previously reported.[22] All data is available in CIF format (CCDC numbers 2011710–2011713).

Deposition Numbers 2011710–2011713) contain the supplementary crystallographic data for this paper. These data are provided free of charge by the joint Cambridge Crystallographic Data Centre and Fachinformationszentrum Karlsruhe Access Structures service www.ccdc.cam.ac.uk/structures.

Acknowledgments

Financial support from the Swedish Research Council, the Knut and Alice Wallenberg Foundation and the Royal Physiographic Society in Lund is gratefully acknowledged.

Keywords: Cross-coupling · Homogeneous catalysis · Nickel · Pincer ligands · Paramagnetic complexes

[1] M. Albrecht, G. van Koten, *Angew. Chem. Int. Ed.* **2001**, *40*, 3750–3781; *Angew. Chem.* **2001**, *113*, 3866.
[2] J. T. Singleton, *Tetrahedron* **2003**, *59*, 1837–1857.
[3] M. E. van der Boom, D. Milstein, *Chem. Rev.* **2003**, *103*, 1759–1792.
[4] D. Morales-Morales, C. M. Jensen (Eds.), *The Chemistry of Pincer Compounds;* Elsevier Science B. V.: Amsterdam, **2007**.
[5] N. Selander, K. J. Szabó, *Chem. Rev.* **2011**, *111*, 2048–2076.
[6] G. van Koten, D. Milstein (Eds.), Organometallic pincer chemistry. *Top. Organomet. Chem.* **2013**, *40*, p. 1.
[7] K. J. Szabó, O. F. Wendt (Eds.), *Pincer and Pincer-Type Complexes*; Wiley-VCH Verlag GmbH & Co. KGaA, **2014**.
[8] G. Bauer, X. Hu, *Inorg. Chem. Front.* **2016**, *3*, 741–765.
[9] H. Valdés, A. García-Eleno Marco, D. Canseco-Gonzalez, D. Morales-Morales, *ChemCatChem* **2018**, *10*, 3136–3172.
[10] M. Gandelman, A. Vigalok, L. J. W. Shimon, D. Milstein, *Organometallics* **1997**, *16*, 3981–3986.

[11] E. Poverenov, M. Gandelman, L. J. W. Shimon, H. Rozenberg, Y. Ben-David, D. Milstein, *Chem. Eur. J.* **2004**, *10*, 4673–4684.
[12] E. Poverenov, M. Gandelman, L. J. W. Shimon, H. Rozenberg, Y. Ben-David, D. Milstein, *Organometallics* **2005**, *24*, 1082–1090.
[13] D. M. Spasyuk, D. Zargarian, A. van der Est, *Organometallics* **2009**, *28*, 6531–6540.
[14] G. R. Fulmer, W. Kaminsky, R. A. Kemp, K. I. Goldberg, *Organometallics* **2011**, *30*, 1627–1636.
[15] J.-L. Niu, X.-Q. Hao, J.-F. Gong, M.-P. Song, *Dalton Trans.* **2011**, *40*, 5135–5150.
[16] B. Mougang-Soumé, F. Belanger-Gariépy, D. Zargarian, *Organometallics* **2014**, *33*, 5990–6002.
[17] W. D. Bailey, L. Luconi, A. Rossin, D. Yakhvarov, S. E. Flowers, W. Kaminsky, R. A. Kemp, G. Giambastiani, K. I. Goldberg, *Organometallics* **2015**, *34*, 3998–4010.
[18] A. Fleckhaus, A. H. Mousa, N. S. Lawal, N. K. Kazemifar, O. F. Wendt, *Organometallics* **2015**, *34*, 1627–1634.
[19] L. S. Jongbloed, D. García-López, R. van Heck, M. A. Siegler, J. J. Carbó, J. I. van der Vlugt, *Inorg. Chem.* **2016**, *55*, 8041–8047.
[20] A. H. Mousa, A. Fleckhaus, M. Kondrashov, O. F. Wendt, *J. Organomet. Chem.* **2017**, *845*, 157–164.
[21] L. S. Jongbloed, N. Vogt, A. Sandleben, B. de Bruin, A. Klein, J. I. van der Vlugt, *Eur. J. Inorg. Chem.* **2018**, *2018*, 2408–2418.
[22] A. H. Mousa, J. Bendix, O. F. Wendt, *Organometallics* **2018**, *37*, 2581–2593.
[23] A. H. Mousa, A. V. Polukeev, J. Hansson, O. F. Wendt, *Organometallics* **2020**, *39*, 1553–1560.
[24] P. L. Arnold, M. S. Sanford, S. M. Pearson, *J. Am. Chem. Soc.* **2009**, *131*, 13912–13913.
[25] F. Kakiuchi, T. Kochi, H. Mutsutani, N. Kobayashi, S. Urano, M. Sato, S. Nishiyama, T. Tanabe, *J. Am. Chem. Soc.* **2009**, *131*, 11310–11311.
[26] T. W. Lyons, M. S. Sanford, *Chem. Rev.* **2010**, *110*, 1147–1169.
[27] a) M. Kondrashov, S. Raman, O. F. Wendt, *Chem. Commun.* **2015**, *51*, 911; b) M. Kondrashov, D. Provost, O. F. Wendt, *Dalton Trans.* **2016**, *45*, 525–531.
[28] M. H. Majeed, P. Shayesteh, P. Tunå, A. R. Persson, R. Gritcenko, L. R. Wallenberg, L. Ye, C. Hulteberg, J. Schnadt, O. F. Wendt, *Chem. Eur. J.* **2019**, *25*, 13591–13597.
[29] D. A. Ahlstrand, A. V. Polukeev, R. Marcos, M. S. G. Ahlquist, O. F. Wendt, *Chem. Eur. J.* **2017**, *23*, 1748–1751.
[30] G. W. Roffe, S. Boonseng, C. B. Baltus, S. J. Coles, I. J. Day, R. N. Jones, N. J. Press, M. Ruiz, G. J. Tizzard, H. Cox, J. Spencer, *R. Soc. Open Sci.* **2016**, 3, https://doi.org/10.1098/rsos.150656.
[31] Y. Wang, C. Qin, X. Jia, X. Leng, Z. Huang, *Angew. Chem. Int. Ed.* **2017**, *56*, 1614–1618; *Angew. Chem.* **2017**, *129*, 1636.
[32] This ligand was previously reported by Huang (ref.[31]). However, the reported ^{31}P NMR chemical shift is more downfield than the value we found; our value is consistent with our previously reported PCN ligands.
[33] D. J. Cárdenas, A. M. Echavarren, M. C. Ramírez de Arellano, *Organometallics* **1999**, *18*, 3337–3341.
[34] During the submission of this manuscript a report on the base induced C–H nickelation of ligand **8** appeared: L. Kletsch, G. Hörner, A. Klein, *Organometallics* **2020**, *39*, 2820–2829.
[35] a) D.-D. Shao, J.-L. Niu, X.-Q. Hao, J.-F. Gong, M.-P. Song, *Dalton Trans.* **2011**, *40*, 9012; b) J.-P. Cloutier, B. Vabre, B. Moungang-Soumé, D. Zargarian, *Organometallics* **2015**, *34*, 133–145.
[36] A. Klein, B. Rausch, A. Kaiser, N. Vogt, A. Krest, *J. Organomet. Chem.* **2014**, *774*, 86–93.
[37] X. Ni, L. Deng, H. Wang, *J. Quant. Spectrosc. Radiat. Transfer* **2017**, *196*, 165–168.
[38] O. Vechorkin, V. Proust, X. Hu, *J. Am. Chem. Soc.* **2009**, *131*, 9756–9766.

Received: July 30, 2020